

Quantitative hydrodynamic investigation of fish caudal fin cupping motion using a bio-robotic model

Kainan Hu, Ziyu Ren, Yueping Wang, Tianmiao Wang, and Li Wen*

Abstract—The three-dimensional deformation of fish caudal fin during swimming was reported in several teleost bony fish species, e.g., bluegill sunfish (*Lepomis macrochirus*) and cichlid fish (*Pseudotropheus greshakei*). However, few study has addressed the effect of 3D locomotion on its thrust efficiency quantitatively. In this paper, we first performed biological observations on yellow perch (*Perca flavescens*) and confirmed the evidence of “cupping” motion for the steady swimming behaviors. The biological kinematics data was then extracted and appropriately programmed into to a robotic caudal fin model coupled with heave and pitch oscillatory motions. We then conducted systematic hydrodynamic experiments on this physical model by manipulating Strouhal numbers ($St=0.16-0.50$). Comparison between the cupping fin motion and the flat motion showed that the thrust force increased by 78% at the St of 0.32, and thrust efficiency increased 16% at the St of 0.28. DPIV experiments in the horizontal plane were conducted at representative experimental scenarios ($St=0.22$ and 0.5). We found that the cupping motion has a significant effect on the wake structure, which was distinct with the typically found wake structure, for example, reversed Karman vortex reported by many two-dimensional flapping foil studies. Quantitative analysis of wake flow further demonstrated that the caudal fin generated stronger vortex circulation with addition of cupping motion. We hypothesize that the fish may control the cupping motion to obtain better swimming efficiency under different swimming states.

I. INTRODUCTION

Traditional underwater vehicles have long been criticized for its poor efficiency and bad maneuverability [1]. As the application of underwater vehicle expanded, there is an increasing demand for the improvement of propulsion devices on efficiency, maneuverability, and stealth to allow for the missions undertaken in more complex environments and for a longer cruise time. Fish outperforms the man-made underwater vehicles for its high efficiency, high maneuverability and high quality of stealth [2] and has become an extraordinary inspiration for underwater vehicle design [3]. One of the most distinct features that differs fish from other aquatic animals is the multiple flexible fins. For ray-finned fishes, these flexible control surfaces are composed of individual ray-like components connected to each other through a collagenous membrane [4]. The muscle at the fin base can be used to bend or tune the flexibility of the fin ray, therefore, achieves the control of the complex 3D fin surface

This work was supported by the National Science Foundation support key projects, China, under contract number 61633004; National Science Foundation support projects, China, under contract number 61403012, National Science Foundation support key projects, China, under contract number 61333016.

The authors are with the School of Mechanical Engineering and Automation, Beihang University, Beijing, 100191, People’s Republic of China; * e-mail for contact: liwen@buaa.edu.cn.

interacting with the fluid environment. Many studies suggest that such active control of the fin surface is essential for fish locomotion [5, 6].

As investigated in excessive biological [7], theoretical [8] and bio-robotic studies [9], the fish caudal fin is the largest source of propulsion force. The caudal fin of the bony fish also possess similar structures as pectoral and dorsal fins and has been observed to conduct complex 3D locomotion during the maneuver and steady swimming [10, 11]. Although the modulation of the caudal fin shape is commonly reported in biological observations, few quantitative studies incorporated such active surface control. Esposito et al. used a robotic caudal fin with six individual actuated fin rays to mimic several different 3D movement patterns of bluegill sunfish. They measured propulsion forces at a fixed flow speed and found 3D caudal fin motion could generate propulsion force deviate the fish body axis, which achieved functional asymmetric on a symmetric tail [12]. Ren et al. further took the peduncle motion and the flow velocity into consideration. They demonstrated that at lower swimming speed, the caudal fin can be used as an effective vectoring propeller [13, 14]. Different from traditional cognitions that modeled the fish tail as a 2D plate during steady swimming, the fish caudal fin tends to form a cup-shape morphology, called cupping motion, instead of stretching to be flat [6, 10, 11]. Based on DPIV results from the live fish, Tytell speculates such movement could improve the utilization rate of the flow and may lead to the hairpin vortex structures behind the caudal fin [6]. However, no quantitative study has supported his speculation yet. The study of Esposito et al. showed the cupping motion would produce larger thrust force [12].

In this paper, we used a robotic caudal fin to help us understand the contribution of the cupping motion to the caudal fin thrust performance. We first performed a series of biological observations on yellow perch (*Perca flavescens*) and confirmed that this kind of fish does tend to cup its tail during steady swimming. The kinematic data from the animal were then mapped to the robotic model to mimic the cupping motion of its biological counterpart. Thrust force, input power and thrust efficiency of three movement patterns were measured under different Strouhal numbers ranging from 0.16 to 0.50 for comparison. Wake flow structures in the horizontal plane were obtained at typical time instants, and quantitative

TABLE I. KINEMATIC DATA OF THREE CAUDAL FIN MOTIONS

Motions	Big Cupping	Small Cupping	Flapping
Excursion(x1, x5)/mm	140	130	125
Excursion(x2, x4)/mm	130	120	125
Excursion(x3)/mm	110	110	125

analysis of the wake was conducted subsequently. In the end, we compared the results to previous works and hypothesized that the fish might perform the cupping motion to achieve large thrust force and high efficiency.

II. MATERIALS AND METHODS

A. Fish

The living fish we used during the experiments were yellow perch, known as *Perca flavescens*, which were purchased from legal fishermen in Shandong, China. Five fish were kept in the freshwater aquarium at about 20°C and fed three times a week. Fish were put into the circular water tank 30 minutes before experiments so that they could adapt themselves to the environment. We euthanized those fish after observing their kinematics in order to obtain morphologic data. The total length of five fish were similar in a proper range: 128 mm ± 4 mm (total length, mean ± s.d.).

B. Biological Experiment

Although many previous studies have reported the cupping motion observed during fish swimming, the kinematic data of the cupping motion is still limited. Biological experiments were carried to extract key parameters including heave and pitch amplitudes of the caudal peduncle, lateral excursions of fin rays and phase lag between the fin ray and the body movement. The experiments were performed in a circular water tank. The flow speed of the tank was adjusted to 2L·s⁻¹, and the videos were recorded only when the fish turned into steady swimming mode. We used two high-speed cameras (FASTCAM Mini UX100, PHOTRON, Japan) to record the movement of caudal fin in posterior view and ventral view respectively. The frame rate of the camera was set to 250 Hz. We then used a commercial software ProAnalyst (Xcitex Inc., USA) to analyze the real fish kinematics. We defined five points to illustrate fin rays' movement shown in Fig. 2(a) and two points to illustrate caudal peduncle movement shown in Fig. 2(b). We assumed the fish swam in the tank horizontally and only lateral excursion of the point was considered in this study.

C. Robotic Caudal Fin Experiment

The robotic caudal fin used in this study was developed based on our previous work [13]. This robotic model allowed each five fin rays to be controlled individually so that they could form various three-dimensional shapes. The robotic caudal fin was connected to a towing system, which can provide towing speed and mimic the peduncle motion (heave & pitch). The strut connected the robotic model and the towing system was carefully adjusted to let the model work in the mid-depth of the tank. The robotic caudal fin was programmed to perform three different motions: (a) big cupping, (b) small cupping and (c) flapping. Kinematic parameters of each movement pattern are shown in Table 1. It should be noted that the small cupping motion was the exact replica of the real fish cupping movement, in which the fin ray amplitude was carefully scaled up. Big cupping motion exaggerated the lateral excursion of four fin rays except the middle fin ray. Besides, the heave & pitch amplitude and the phase lag was set as 17mm, 13° and 90° respectively.

Robotic experiments were conducted under a series of Strouhal numbers (St) ranging from 0.16 to 0.50. St is a dimensionless number that describes the swimming performance of aquatic animals. It can be defined by the following equation [15]:

$$St = \frac{f \times A}{U} \quad (1)$$

where f , A and U represented the frequency, the heave amplitude and the flow speed respectively. By varying the towing speed U , we changed St with an interval of 0.20. Particularly, the span of St fully covered the optimal St for fish swimming [16].

The force transducer (mini-40, ATI Industrial Inc., Canada) was mounted between the robotic model and the towing system (see Fig. 1). In each trial, the hydrodynamic force would be recorded in real time and subsequently be used to calculate the thrust force and the input power. The input power P and efficiency η of the robotic caudal fin were defined as:

$$P = P_{heave} + P_{pitch} = \frac{\int_0^T |F_{heave_z} \times V_{heave_z}| dt}{T} + \frac{\int_0^T |\tau_{z_1} \times V_{pitch_1}| dt}{T} \quad (2)$$

$$\eta = \frac{P_{out}}{P_{in}} = \frac{TF \times U}{P - P_{mec}} \quad (3)$$

where V , τ_z , TF and U represented peduncle speed, torque along the z-axis, thrust force and towing speed respectively. P_{mec} was the mechanical loss of the model and should be subtracted from the total power input. It was measured by running the model in the air.

The method we used in this study to evaluate the wake flow structure is digital particle image velocimetry (DPIV). We seeded the near-neutrally buoyant glass beads with a diameter of 20 μm evenly into the water and illuminated the particles with a laser sheet with the thickness of 1.5 mm. The laser sheet was carefully adjusted to project horizontally and to sweep the mid fin ray endpoint of the caudal fin model (see Fig. 1). The movement of the particles were recorded by a high-speed camera (SP5000, JAI Inc., Denmark) with the sampling rate of 250 Hz. We assumed that there is no

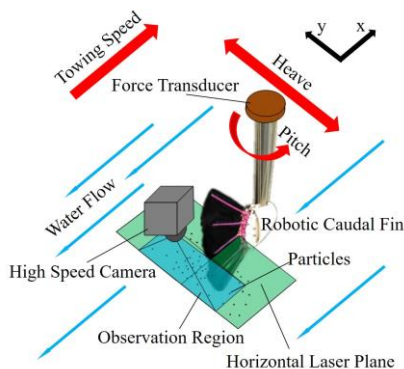


Figure 1. Robotic experiment setup. All apparatus were towed by a guide rail system at a given speed. Heave and pitch motions were programmed to simulate caudal peduncle motion of real fish. Force Transducer was mounted at the connection between the caudal fin and the towing system that generates peduncle motion. A high-speed camera recorded the movement of particles which were illuminated by a laser sheet. The laser sheet was about 1mm thick and was projected horizontally on the middle fin ray. Please refer to our previous work for more details of the experimental setup. [13]

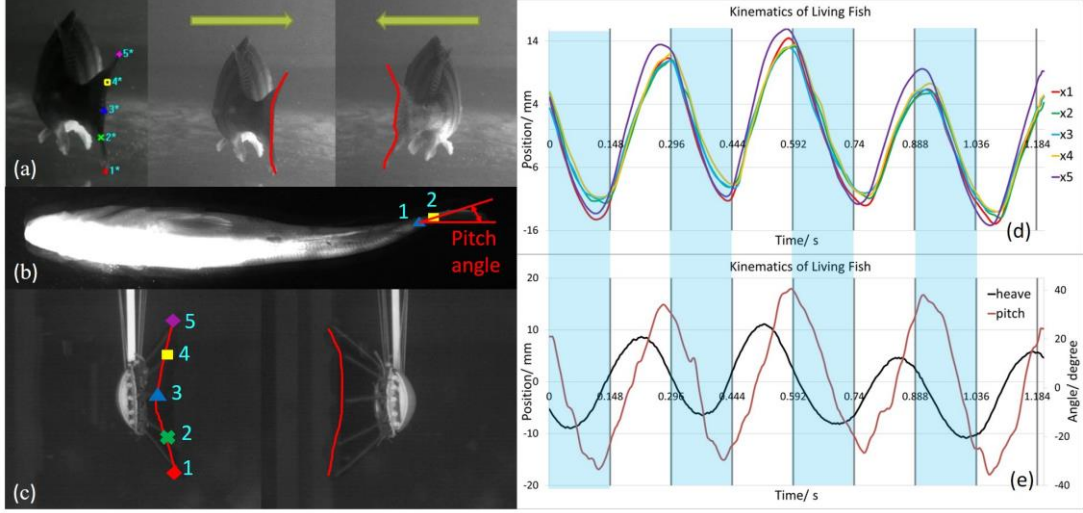


Figure 2. Posterior view of the fish. Five points along caudal fin trailing edge were selected to identify the three-dimensional motion: Point 1 (red) was the end of the bottom fin ray, Point 2 (green) was the end of the fourth fin ray down from the middle fin ray, Point 3 (blue) was the end of the middle fin ray, Point 4 (yellow) was the end of the fourth fin ray up from the middle fin ray and Point 5 (purple) was the end of the top fin ray. (b) Ventral view of the fish. Two points of the body were selected to identify its peduncle motion: Point 1 (blue) at caudal peduncle and Point 2 (yellow), 5 mm behind Point 1 along the body midline. The excursion of Point 1 denoted heave amplitude. The angle between the horizontal line and the connection line between point 1 and point 2 denoted pitch angle. (c) Posterior view of robotic caudal fin during cupping motion. Five fin ray endpoints matched that of living fish. (d) Kinematic data of fish's five fin rays at flow speed $2L \cdot s^{-1}$. (e) Kinematic data of fish's caudal peduncle at flow speed $2L \cdot s^{-1}$. See supplementary Video 1.

shearing motion between the particle and the surrounding fluid, hence the velocity of the particle was considered to be the velocity of the flow field at that point. The velocity vector field in observation region can be obtained by conducting cross-correlation to the high-speed image sequences.

Since the force and the wake structure are closely connected in unsteady propulsion, the concept of circulation is incorporated to evaluate the of thrust force [17], and this method has been widely used in previous research [2, 18, 19]. In this method, the circulation of a vortex was calculated:

$$\Gamma = \oint_C v_t dx \quad (4)$$

where dx and v_t were the differential element and the tangential velocity along curve C , respectively. The vortex always occurred at the area that has large velocity gradient, i.e., the region with large vorticity. The velocity field was obtained by conducting the following calculation:

$$\text{vorticity} = \nabla \times \vec{v} = \begin{vmatrix} i & j & k \\ \frac{\partial}{\partial x} & \frac{\partial}{\partial y} & \frac{\partial}{\partial z} \\ u & v & w \end{vmatrix} \quad (5)$$

where u and v were velocity along x -axis and y -axis respectively. w was 0 since the velocity field was limited in a 2D plane. We then can pinpoint the position of a vortex according to its vorticity magnitude.

III. RESULTS

A. Biological Observation

Lateral excursions of five points along the fish caudal fin trailing edge were shown in Fig. 2(d). The excursion data showed that all five points' movements can be expressed as a trigonometric function:

$$y = A \sin(2\pi ft + \phi) \quad (6)$$

where A was the unilateral amplitude of the excursion, f was the frequency and ϕ was the phase lag. The frequency of each point was around 3Hz , and there was no phase lag between all five points. Excursion of five points differed from each other. The minimal excursion occurred at the middle fin ray with 20mm, while the maximal excursion took place at the top fin ray with 25mm, 25% more than the minimum one.

The movement of the peduncle can also be expressed as a trigonometric function. The phase lag between the heave and pitch was exactly 90° . When comparing peduncle data to fin ray data, we found out that heave motion leads excursion with a phase lag of 90° , which means there was no phase lag between pitch motion and excursion.

B. Thrust Force and Efficiency

Two cupping motions generated stronger thrust force than flapping motion in most cases. Average excursion of small cupping was 120mm, which was smaller than flapping motion (125mm). However, the forces of small cupping were continuously higher than cupping motion from $St=0.3$ to 0.5. When it came to St below 0.3, force magnitude of small cupping and flapping surpassed each other alternately. It was noticeable that the thrust force of small cupping was 1.78 times as much as flapping at $St=0.32$. Within the optimal St for fish swimming, small cupping thrust force was near or stronger than flapping under smaller average lateral excursions. Average excursion of big cupping was 126mm, slightly greater than flapping but its thrust force was remarkably greater than flapping in majority cases. At St 0.28, big cupping thrust force exceeded flapping more than 55%.

The thrust efficiencies of three motion patterns were summarized in Fig. 4. Small cupping and flapping indicated a similar tendency: drastic augmenting first, then falling down and tending to keep steady in the end. However, the thrust

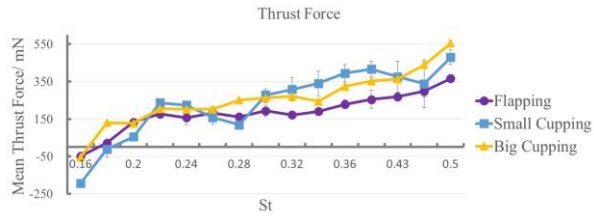


Figure 3. Mean thrust force of three motion patterns: flapping, small cupping and big cupping under different St ranging from 0.16 to 0.5 during one flapping cycle.

efficiency of big cupping kept fluctuating after reaching its maximum. St correspond to the highest efficiency has changed: flapping: 0.20 (71%), small cupping: 0.22(66%) and big cupping: 0.22(64%). Besides, the position that thrust efficiency changed from negative to positive had moved. It should be noted that the majority points of each motion located around distinct efficiency numbers: flapping: 40%, small cupping: 30%, big cupping: 50%.

We summarized the findings as follows:

(i) Thrust efficiency of small cupping can be obtained as the same magnitude as flapping under many St while its thrust force could be near 1.78 times than that of flapping. Furthermore, when small cupping efficiency were much lower than flapping, its thrust force can reach or be little higher than that of flapping nevertheless.

(ii) The thrust efficiency of big cupping was not sensitive to the variation of flow speed. It raised thrust efficiency and thrust force constantly from St 0.28 to 0.4 at the same time, comparing to flapping motion. Especially, At St 0.28, the thrust efficiency increased 16% while thrust force increased by 55%. Within St 0.22 to 0.26, though the thrust efficiency of big cupping are low, the thrust force were higher.

(iii) Big cupping thrust efficiency was either close to small cupping or higher than it. But big cupping decreased thrust force sometimes. Oscillation of big cupping efficiency was clearly minor than small cupping.

C. Wake structure evaluation

Although the cupping motion dominated the flapping motion respect to thrust force within a wide Strouhal number range, its thrust efficiency only superior to the flapping motion within some narrow ranges (see Fig. 3 and 5). The DPIV was conducted at $St=0.22$ and 0.50, where the thrust efficiency of the big cupping motion reached the highest and stable value respectively. Since the caudal fin would reach maximum lateral displacement and shed vortex from the trailing edge at $0.5T$ and T in both cupping and flapping motion, we chose the wake structures at these two time instants for demonstration. We also marked out the vortices in each case that may link into a vortex ring based on its vorticity magnitude and the jet flow direction (see Fig. 5 and 6). For example, in Fig. 5d, since Vortex 1 and 2 had similar vorticity magnitude, and a clear current passed through the vortex pair, these two vortices were supposed from the same vortex ring structure. While the vortex indicated by color blue near the Vortex 2 was too weak and hence be overlooked in this study. Besides, although the vorticity magnitude of the

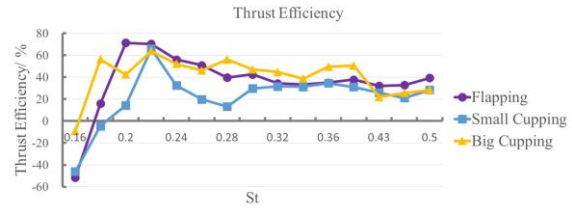


Figure 4. Thrust efficiency of three motion patterns: flapping, small cupping and big cupping under different St ranging from 0.16 to 0.5 during one flapping cycle.

vortex indicated by color red below the Vortex 2 was large, the jet direction between these two vortices was too deflected from the thrust direction, which we assumed had less effect on the thrust performance and hence left it out.

When moving the robotic caudal fin with flapping motion at $St=0.50$, the typical wake structure that similar to the reversed Karman vortex street was observed (see Fig. 5a and 6b). However, such wake structure was hardly being observed in cupping motion. When the new forming vortex just shedding from the trailing edge, three vortices with opposite rotating direction followed and totally three jet flows would form between the downstream vortices and the new forming one (see Fig. 5c and 6d). This structure is similar to the discovery that reported by [9]. The flow downstream is much more parallel to the x direction, which is different from that in flapping motion that the flow would be directed to one side. When we decrease St to 0.22 by increasing the towing speed, the wake structure of these two movements changed slightly (see Fig. 6).

In general, the jet angle in cupping motion (average absolute jet angle was 31.9° at $St=0.22$ and 36.2° at $St=0.50$) was larger than that in flapping motion (average absolute jet angle was 30.1° at $St=0.22$ and 30.4° at $St=0.50$), especially at $St=0.50$. That means with cupping motion, the robotic caudal fin directed more water laterally, which was unfavorable to boost thrust efficiency. At $St=0.22$, the jet angle of the cupping motion was close to flapping motion, suggesting the thrust efficiency of these two motion should be close. At $St=0.50$, the jet angle gap between cupping and flapping increased, suggesting the difference between the thrust efficiency should increase. Besides, the vortices formed by cupping was larger and stronger than that formed by flapping in general, especially when $St=0.50$ (see average interval and average circulation in Table 2), suggesting the cupping motion would generate larger thrust force as shown in Fig. 3. In flapping motion, it seems that the average absolute jet angle did not change much when St changed from 0.22 to 0.50 (increased by only 1%). However, the average circulation decreased dramatically (declined by 24%). Things were different for cupping motion, where the average absolute jet angle increased significantly (increased by 14%) while the average vortex circulation kept stable (enhanced by 5%).

IV. DISCUSSION AND CONCLUSION

Our biological experiments demonstrate that yellow perch would perform apparent cupping movement during steady swimming at high speed ($2Ls^{-1}$). The wide observation of the cupping motion reminds us that it is insufficient to

regard the fish tail as a simple 2D plate even when fish is performing steady swimming.

The discoveries in this study confirmed some conjectures and findings in previous research. Esposito et al. shows the cupping motion could achieve higher thrust force at different motion frequency and fin ray stiffness comparing to other movement patterns. This study may be the first quantitative investigation that demonstrates the cupping motion is superior in thrust generation. However, since all the tests were conducted at the same flow speed, we still couldn't figure out whether the cupping motion is superior under the

different Strouhal number. According to our results, the thrust force produced by both small and big cupping motion was larger than that of flapping motion at St ranging from 0.22 to 0.50, in general. However, different cupping motion possessed different thrust performance. Small cupping motion performed well when St ranged from 0.30 to 0.43, while the big cupping motion outperformed it within other St ranges. Some argue that cupping can enhance thrust due to the variation of the caudal fin height that leads to the change of the tail area encountering the water flow. In this process, the caudal fin reaches the maximum height near the midway

TABLE II. WAKE STRUCTURE DATA OF TWO MOTION PATTERNS

Movement pattern	Strouhal number	Time instant	Jet	Jet angle θ_{ij} (deg)	Average absolute jet angle(deg)	Vortex interval D_{ij} (mm)	Average interval(mm)	Average circulation C_{ij} (mm^2s^{-1})	Average circulation(mm^2s^{-1})
Cupping	0.22	0.5T	J12	-46.2	31.9	53.3	74.1	1888.6	1996.9
			J13	-26.5		87.5		1743.4	
			J14	-28.2		75.2		1531.5	
		T	J12	21.6		88.8		2013.3	
			J13	28.0		88.6		2293.5	
			J14	40.9		51.1		2511.1	
	0.50	0.5T	J12	-44.9	36.2	50.3	63.8	1866.5	2105.8
			J13	-35.1		63.6		2408.6	
			J14	-28.8		78.2		1779.3	
		T	J12	28.8		84.4		1942.1	
			J13	31.8		63.1		2166.9	
			J14	47.9		43.4		2471.5	
Flapping	0.22	0.5T	J12	-36.4	30.1	75.3	73.1	2855.6	2151.1
			J23	20.5		53.3		2286.8	
		T	J12	35.2		81.5		2009.8	
			J23	-28.3		82.4		1452.1	
	0.50	0.5T	J12	-39.4	30.4	65.6	55.5	2564.2	1640.2
			J23	16.9		45.3		1570.0	
		T	J12	25.6		71.8		1553.7	
			J23	-39.6		39.3		872.6	

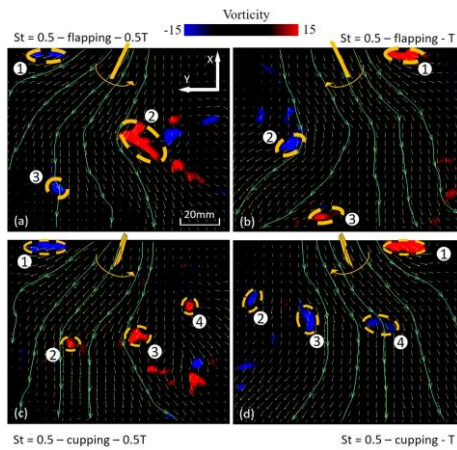


Figure 5. Instantaneous PIV results of flapping and big cupping at 0.5T and T when $St = 0.5$. Caudal fin position, coordinate system, scale and streamlines were displayed. Important vortices were labeled in sequence.

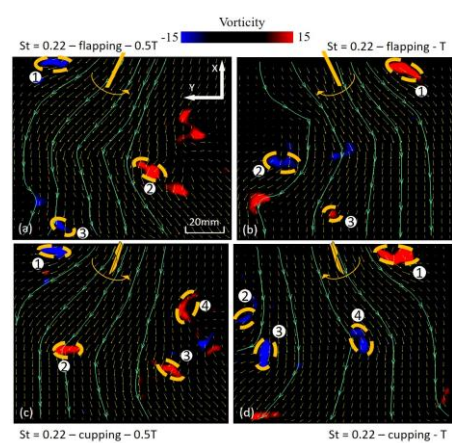


Figure 6. Instantaneous PIV results of flapping and big cupping at 0.5T and T when $St = 0.22$. Caudal fin position, coordinate system, scale and streamlines were displayed. Important vortices were labeled in sequence.

between maximal lateral excursion and the minimum height near the maximum excursion [11].

The thrust efficiency is another important factor to evaluate the propulsion performance. Tytell has mentioned the advantage of the cupping motion in his study on fish median fins [6]. He pointed out that fish tail may not as efficiency as a 2D plate because some part of the flow near the tail tip may be pushed up and down and generated momentum that cancels out. The cupping motion may be an attempt to reduce this effect. Our study confirmed that cupping motion does enhance the thrust efficiency within some St extents, while, a suitable cupping amplitude is also critical. For example, the big cupping motion was more efficient than flapping motion with St ranging from 0.28 to 0.40. However, the performance of small cupping motion was even poorer than flapping. We also compare the efficiency measured in our experiments to results obtained in previous experimental and numerical studies on 2D flapping foils. The maximum efficiency achieved by our robotic caudal fin is significantly higher than the efficiency reported in these studies [20,21].

Tytell has hypothesized that the bluegill sunfish may shed vortex with the morphology like hairpin [6]. Previous CFD study also found similar structures in flexible fin [21]. In this paper, we found the wake structure of the cupping motion was much more different from that of the flapping motion and resemble the morphology proposed by Tytell (see Fig. 12 in [6]). We confirm that the cupping motion is the leading cause of the hairpin vortex. By performing the cupping motion, the velocity of each point along the caudal fin trailing edge is different, which lead to the vortex shed from various position does not detach the trailing edge at the same time. The wake structure of both cupping and flapping motion increased in size when St reduced, while, the absolute jet angle and the average circulation showed different variation tendency. Taking it by and large, the change of the St had more significant effect on jet angle than circulation for cupping motion. For flapping motion, the conclusion reversed. The large magnitude of the vortex circulation within a wide St range may be critical for cupping motion to generate larger thrust force than flapping motion. The cupping motion's low efficiency at high St values may attribute to the large jet angle which suggests that more water was pushed laterally and hence wasted more input energy.

At certain swimming speeds and adopting appropriate cupping motion, the fish could obtain larger thrust force and higher efficiency. However, when the circumstance becomes unfavorable, it may actively control the caudal fin rays and apply other movement patterns such as flapping to achieve high-efficient swimming. In the future, we will continue working on uncovering the mystery of the fish tail 3D motion with the aid of CFD to predict the thrust efficiency and wake flow structure of the cupping motion theoretically and go in depth the generation mechanism of wake flow structure observed in robotic experiments.

ACKNOWLEDGMENT

This work was supported by the National Science Foundation support projects, China, under contract number

61403012, National Science Foundation support key projects, China, under contract number 61333016, and National Science Foundation Key grant contract number 61633004 to Li Wen.

REFERENCES

- [1] M. Sfakiotakis, D. M. Lane, and J. B. C. Davies, "Review of fish swimming modes for aquatic locomotion," *Oceanic Engineering, IEEE Journal of*, vol. 24, pp. 237-252, 1999.
- [2] L. Wen, T. M. Wang, G. H. Wu, and J. H. Liang, "Quantitative Thrust Efficiency of a Self-Propulsive Robotic Fish: Experimental Method and Hydrodynamic Investigation," *Ieee-Asme Transactions on Mechatronics*, vol. 18, pp. 1027-1038, Jun 2013.
- [3] Q. Shen, T. M. Wang, J. H. Liang, and L. Wen, "Hydrodynamic performance of a biomimetic robotic swimmer actuated by ionic polymer-metal composite," *Smart Materials and Structures*, vol. 22, Jul 2013.
- [4] S. Alben, P. G. Madden, and G. V. Lauder, "The mechanics of active fin-shape control in ray-finned fishes," *J R Soc Interface*, vol. 4, pp. 243-56, Apr 22 2007.
- [5] B. E. Flammang and G. V. Lauder, "Functional morphology and hydrodynamics of backward swimming in bluegill sunfish, *Lepomis macrochirus*," *Zoology*, 2016.
- [6] E. D. Tytell, "Median fin function in bluegill sunfish *Lepomis macrochirus*: streamwise vortex structure during steady swimming," *J Exp Biol*, vol. 209, pp. 1516-34, Apr 2006.
- [7] C. D. Wilga and G. V. Lauder, "Biomechanics: hydrodynamic function of the shark's tail," *Nature*, vol. 430, p. 850, Aug 19 2004.
- [8] M. Lighthill, "Aquatic animal propulsion of high hydromechanical efficiency," *Journal of Fluid Mechanics*, vol. 44, pp. 265-301, 1970.
- [9] T. Wang, L. Wen, J. Liang, and G. Wu, "Fuzzy vorticity control of a biomimetic robotic fish using a flapping lunata tail," *Journal of Bionic Engineering*, vol. 7, pp. 56-65, 2010.
- [10] B. E. Flammang and G. V. Lauder, "Caudal fin shape modulation and control during acceleration, braking and backing maneuvers in bluegill sunfish, *Lepomis macrochirus*," *J Exp Biol*, vol. 212, pp. 277-86, Jan 2009.
- [11] B. E. Flammang and G. V. Lauder, "Speed-dependent intrinsic caudal fin muscle recruitment during steady swimming in bluegill sunfish, *Lepomis macrochirus*," *J Exp Biol*, vol. 211, pp. 587-98, Feb 2008.
- [12] C. J. Esposito, J. L. Tangorra, B. E. Flammang, and G. V. Lauder, "A robotic fish caudal fin: effects of stiffness and motor program on locomotor performance," *J Exp Biol*, vol. 215, pp. 56-67, Jan 1 2012.
- [13] Z. Ren, X. Yang, T. Wang, and L. Wen, "Hydrodynamics of a robotic fish tail: effects of the caudal peduncle, fin ray motions and the flow speed," *Bioinspiration & Biomimetics*, vol. 11, p. 016008, 2016.
- [14] Z. Ren, K. Hu, T. Wang, and L. Wen, "Investigation of Fish Caudal Fin Locomotion Using a Bio-inspired Robotic Model," 2016.
- [15] J. Anderson, K. Streitlien, D. Barrett, and M. Triantafyllou, "Oscillating foils of high propulsive efficiency," *Journal of Fluid Mechanics*, vol. 360, pp. 41-72, 1998.
- [16] C. Eloy, "Optimal Strouhal number for swimming animals," *Journal of Fluids and Structures*, vol. 30, pp. 205-218, Apr 2012.
- [17] M. H. Dickinson, "Unsteady mechanisms of force generation in aquatic and aerial locomotion," *American Zoologist*, vol. 36, pp. 537-554, 1996.
- [18] G. Wu, Y. Yang, and L. Zeng, "Kinematics, hydrodynamics and energetic advantages of burst-and-coast swimming of koi carps (*Cyprinus carpio koi*)," *J Exp Biol*, vol. 210, pp. 2181-91, Jun 2007.
- [19] U. K. Müller, B. L. E. van den Heuvel, E. J. Stamhuis, and J. J. Videler, "Fish foot prints: morphology and energetics of the wake behind a continuously swimming mullet (*Chelon labrosus* Risso)," *Journal of Experimental Biology*, vol. 200, pp. 2893-2906, 1997-11-01 00:00:00 1997.
- [20] J. J. ALLEN, "Thrust efficiency of harmonically oscillating flexible flat plates," *J. Fluid Mech*, vol. 674, pp. 43-66, 2011.
- [21] Q. Zhu and K. Shoele, "Propulsion performance of a skeleton-strengthened fin," *J Exp Biol*, vol. 211, pp. 2087-100, Jul 2008.